Published in final edited form as:
Cell Mol Bioeng. 2014 March ; 7(1): 1–14. doi:10.1007/s12195-013-0317-4.

Measurement science in the circulatory system

Casey M. Jones[1,2], **Sandra M. Baker-Groberg**[1], **Flor A. Cianchetti**[1], **Jeremy J. Glynn**[1], **Laura D. Healy**[3], **Wai Yan Lam**[1], **Jonathan W. Nelson**[4], **Diana C. Parrish**[5], **Kevin G. Phillips**[1], **Devon E. Scott-Drechsel**[1], **Ian J. Tagge**[1,6], **Jaime E. Zelaya**[1], **Monica T. Hinds**[1], and **Owen J.T. McCarty**[1,3,7]

[1]Department of Biomedical Engineering, Oregon Health & Science University, Portland OR

[2]Department of Chemistry, Lewis & Clark College, Portland OR

[3]Department of Cell & Developmental Biology, Oregon Health & Science University, Portland OR

[4]Division of Cardiology, Knight Cardiovascular Institute, Oregon Health & Science University, Portland OR

[5]Department of Physiology & Pharmacology, Oregon Health & Science University, Portland OR

[6]Advanced Imaging Research Center, Oregon Health & Science University, Portland OR

[7]Division of Hematology & Medical Oncology, Oregon Health & Science University, Portland OR

Abstract

The dynamics of the cellular and molecular constituents of the circulatory system are regulated by the biophysical properties of the heart, vasculature and blood cells and proteins. In this review, we discuss measurement techniques that have been developed to characterize the physical and mechanical parameters of the circulatory system across length scales ranging from the tissue scale (centimeter) to the molecular scale (nanometer) and time scales of years to milliseconds. We compare the utility of measurement techniques as a function of spatial resolution and penetration depth from both a diagnostic and research perspective. Together, this review provides an overview of the utility of measurement science techniques to study the spatial systems of the circulatory system in health and disease.

Introduction

Novel tools and measurement techniques with varying degrees of sensitivity and resolution have been extensively used to define the physical parameters of the circulatory system during homeostasis and in the pathological state. These tools have been implemented both *in vivo* and *ex vivo* with resolution ranging between nanometers and centimeters (Figure 1). In this review, we discuss the utilization of measurement science techniques to define the dynamical role of the cellular and molecular constituents of the circulatory system in regulating organ physiology. We divided the study of the circulatory system into three levels; organs, vessels, and cells. We start out by describing the physical and mechanical characteristics of the circulatory system in health, and where appropriate, how these parameters change in a pathological setting. We then discuss measurement tools that have been used to study each component of the circulatory system at various levels of resolution.

Correspondence: Casey M. Jones, Department of Chemistry, Lewis & Clark College, Portland OR; caseyjones@lclark.edu.

Conflict of Interests

The authors declare no competing financial interests.

This review article was a collaborative effort by the members of the Cardiovascular Working Group at the Oregon Health & Science University. The tools and measurement techniques that were included were in part based on the expertise of the members of the working group, are thus are not inclusive of all the techniques available to the field.

Part I: Organ Physiology and Measurement Tools

1.1. Heart Function

The heart is the central organ of the cardiovascular system. Normal heart function is partially dependent on proper spatial and temporal electrical conduction. The heartbeat is initiated by the firing of Purkinje cells in the sino-atrial node (1). Electrical impulses are propagated through the Purkinje fibers to the atrio-ventricular node, which subsequently travel through the ventricles of the heart. Cardiac myocytes, which receive signals from both Purkinje fibers and adjacent myocytes, respond to depolarization by contracting in sequence to propel blood out of the atrium to the ventricle and into circulation. Heart rate, force of contraction, and speed of repolarization are modulated by neurotransmitter release from sympathetic and parasympathetic nerves that innervate the atria and ventricles (2). An electrocardiogram (ECG) measures heart rate and provides visualization of electrical impulse conduction through the heart. Normal adult human heart rates range from 60–100 beats per minute. Heart rates outside this range may be indicative of any number of pathological conditions, including but not limited to heart failure, myocardial infarction, sepsis, or peripheral vascular abnormalities (3).

Normal blood pressure in humans is considered to be between 100/60 and 120/80 (systolic/diastolic pressure). Blood pressures between 120/80 and 130/90 are categorized as prehypertensive, while blood pressures over 130/90 are categorized as hypertensive. Stroke volume, or the amount of blood pumped from the ventricle with each beat, varies considerably from person to person. Normal stroke volumes range between 55 and 100 mL, with men generally having higher stroke volumes than women. Stroke volumes below 55 mL are indicative of heart failure, while stroke volumes over 100 mL may be indicative of intense and prolonged exercise training (4). A myocardial infarction (MI) occurs when an artery that supplies blood to the heart muscle becomes occluded, either by a blood clot or an arterial plaque. Following a myocardial infarction, the myocardium undergoes significant remodeling, often with pathological consequences, regardless of whether or not the occluded vessel is reperfused. Post-MI remodeling can include fibrosis of heart tissue, infarct expansion, ventricular dilation and wall thinning, and dispersion of repolarization (5). All of these outcomes, alone or in combination, contribute to mortality following MI by increasing the chances of ventricular rupture, heart failure, fatal arrhythmias or sudden cardiac death.

1.2. Measurement Tools

Heart structure and function in both normal and pathological conditions are routinely examined using a variety of imaging modalities in both research and diagnostic settings (6). In this section of the review, we will discuss the following measurement tools: ECG, ultrasound (US) imaging, X-ray computed tomography (CT) imaging, positron emission tomography (PET) imaging, and magnetic resonance imaging (MRI).

1.2.1. Electrocardiography—ECG is perhaps the least expensive and simplest of the methods used to detect heart abnormalities associated with MI, pulmonary embolism, heart murmurs, dysrhythmias, seizures and syncope (7). Electrodes placed on the patient's body measure the electrical signals produced by the heart during each cardiac cycle. While the placement and number of electrodes used may vary depending on application, generally 12 electrodes are used during an ECG exam. Additional electrodes may be added, thus

increasing coverage of the heart and improving the ability to detect MI. The result is a graph ("lead") that traces the cardiac cycle and allows for identification of electrical abnormalities. The trace of a single cycle is split into segments based on peaks and valleys. Irregularities in specific segments of the cardiac cycle correspond to injury in specific areas of the heart and can thus indicate the exact nature of the damage. For instance, ST-segment elevation is a hallmark irregularity indicative of MI (8). While indispensable as a first-look and early-diagnosis tool, ECG is not capable of monitoring blood flow or cardiac pumping ability, and thus injury to some regions of the heart can be missed. Further, ECG is a non-imaging modality, thus is of limited utility in assessment of structural abnormalities.

1.2.2. Ultrasound Imaging—Ultrasound is used as a noninvasive diagnostic tool to assess structure and function within the cardiovascular system. Echocardiography (commonly referred to as 'echo') uses ultrasound to characterize cardiac structure and function. This technique utilizes a transducer that is held against the skin and emits ultrasound waves that travel through blood and soft tissue. The ultrasound waves scatter and bounce back when they encounter dense tissue. The deflected ultrasound waves are collected by the transducer and digitized to a real-time image to reveal structural information. Denser tissues will deflect more ultrasound and will be represented on the image with a brighter pixel. Echocardiography can be used to construct planar images of the heart, 3D volumes, and when used in conjunction with Doppler, measure flow patterns in the heart. Echocardiography is often used to measure cardiac volumes, monitor wall motion, evaluate valve and intracardiac masses, and identify structural defects (9). These measurements use ultrasound frequency ranges between 2 and 18 MHz, with the standard 10 MHz instrument resulting in a longitudinal resolution of 150 μm at a frame rate between 15 and 40 frames per second, thus allowing for detection of movement. Higher frequencies result in increased spatial resolution; however, the depth of penetration decreases with higher frequencies. Doppler ultrasound is a type of ultrasound imaging that reveals information on the flow of blood within the chambers of the heart. During Doppler ultrasound imaging, ultrasound waves strike moving blood cells and are reflected back to the transducer. The frequency of the returning wave is modulated by the direction and velocity of blood flow according to the Doppler Effect. This information can be displayed graphically with spectral Doppler or, more commonly in medical applications, as a color image with a gradient color map corresponding to blood flow rate.

1.2.3. X-ray Computed Tomography and Positron Emission Tomography—CT imaging produces a 3D anatomical image using x-ray images and advanced computation (10). The temporal resolution of CT is between 100–300 ms; total scan times vary based on the use of contrast agent and the number of scans performed. The spatial resolution of CT is 1–5 mm (comparable to MRI, yet with slightly lower resolution); the spatial resolution of PET is between 1–5 cm. 3D volumes are comprised of individual slices that are acquired in the axial plane; processing techniques often can re-slice volumes in a number of orientations depending on actual acquisition details. Computed tomography angiography specifically measures blood flow rate and is used to image coronary artery anatomy, often detecting non-obstructive atherosclerotic plaques even before a level of hemodynamic significance is reached.

PET is a nuclear medical imaging technique. A positron-emitting radionuclide tracer (generally administered intravenously or via inhalation) indirectly emits gamma rays that are subsequently detected in pairs to create a 3D image. The kinetic energy of the positron and the spatial resolution of each of the detectors limit the spatial resolution of PET imaging in humans to 1–2 mm. Because the tracer is attached to a biologically active molecule, PET images represent a biological (often metabolic) process within the body. In order to generate anatomical images, PET must be used in combination with MRI or CT because the tracer is

the signal molecule. Most modern scanners acquire CT and PET images in the same session – PET for (metabolic) functional imaging and CT for anatomical and morphological imaging. PET data is then overlaid on the CT data to ascertain the functional significance via metabolic rate in the location of interest. While ^{18}F-fluorodeoxyglucose is the most prolific radiotracer in PET examinations, a wide variety of tracers have been developed to detect unstable atherosclerotic plaques and to measure myocardial perfusion and metabolism. Though not currently available commercially, development of PET-MRI scanners is an active and promising area of research (11).

PET is regarded as the gold standard technique for non-invasively quantifying myocardial blood flow and has been well validated in animal models of heart function following both reperfused and non-reperfused myocardial infarction (12), as well as in humans at rest and during hyperemia induced by bipyridamole stress (13). Quantification of myocardial blood flow and perfusion is essential in assessing myocardial infarction.

1.2.4. Magnetic Resonance Imaging—Cardiac MRI assesses both structural and functional features within a single examination. MRI is used to generate high-resolution 3D anatomical images to measure heart (and vessel) wall thickness in both healthy and diseased tissues. Single images can be acquired on the order of 20–200 ms. Acquisition of all desired images in a study generally requires ~30 mins. This non-invasive method can be used to measure wall thickening or atrophy due to disease as well as structure changes following treatment (6). Measurement of absolute tissue water-proton (^{1}H) longitudinal relaxation times (T_1, relaxation time in seconds) enables identification of acute myocardial infarction. Parametric maps produced by voxel-by-voxel fitting of T_1 (or R_1 ($\equiv 1/T_1$)) provides a tool to measure the extent and location of the infarct. Exogenous, non-irradiating contrast reagents provide a tool for physicians to study the structure and integrity of the vasculature based upon pharmacokinetic modeling of permeability (14). Contrast-enhanced MRI can detect more morphological details than standard MRI, with the expected detection limits around 0.3 cm^2 (2 × 2 pixels) and 0.5 cm^2 (3 × 4 pixels), respectively. Gadolinium-based contrast reagents administered intravenously are known to transiently extravasate from the blood into the interstitium. Pharmacokinetic modeling of the extravasation rate quantitatively measures vessel permeability (15–18). Further, uptake of contrast reagents into tissue is indicative of deleterious processes such as scarring, infarct, or necrosis. Recent studies have shown that measuring MRI signal enhancement in the heart following cardiac infarct allows for prediction of tissue viability and overall capacity for recovery. Cine imaging, where ECG is utilized to trigger the collection of a series of segmented images, is widely used clinically to observe heart function throughout the entire cardiac cycle (19). Post-processing and advanced modeling techniques quantitatively measure such diagnostically relevant properties including flow, valve ejection rate, strain rates, and ventricular volume. Cardiac MRI has also shown promise as an alternative to PET for quantifying myocardial blood flow and perfusion, which is of both diagnostic and prognostic importance when treating myocardial infarction.

Part II: Vessel Physiology and Measurement Tools

2.1. Blood Vessel Physiology

The human vascular system facilitates the transfer of nutrients and metabolites throughout the entire body. A 70 kg man has approximately five liters of blood and a total vascular surface area of 30–70 m^2 depending on the subject's current activity level (20). Blood flow is driven by a pressure gradient which, in a healthy individual's systemic circulation, pulses between 80–120 mmHg in the arteries and is near zero in the right atrium. A large drop in pressure occurs in the arterioles, vessels 20–80 μm in diameter, which are the next set of smaller blood vessels stemming from arteries, which are 0.1–3 cm in diameter. The diameter

of an arteriole is largely dictated by the extent of arteriolar smooth muscle contraction, which is regulated by a number of local and circulating factors. Changes in arteriolar diameter regulates vessel resistance and the corresponding flow rate through the vessel (21). Although blood flow is typically unidirectional and laminar, vascular branching and atherosclerotic plaques can result in flow separation and recirculation.

2.1.1. Endothelial Cell Physiology—The luminal surface of blood vessels is lined with a confluent monolayer of endothelial cells (ECs). As the interface between the blood and other organs, ECs integrate multiple physical and biochemical cues to regulate platelet adhesion and activation, leukocyte adhesion and transmigration, vascular permeability, vascular tone, and angiogenesis (22, 23). ECs locally mediate these processes through both membrane-bound factors, such as tissue factor, thrombomodulin, and E-selectin, as well as secreted factors, such as nitric oxide and prostacyclin (24). A major determinant of the EC phenotype is the local hemodynamic environment. Wall shear stress resulting from blood flow through the vessel initiates EC cytoskeletal remodeling and causes cellular elongation and alignment in the direction of flow (25). ECs respond to unidirectional, laminar flow by producing numerous factors which inhibit blood platelet recruitment and activation, intimal proliferation and leukocyte adhesion. Conversely, disturbed flow conditions which yield a low average wall shear stress promote EC dysfunction and facilitate the early stages of atherogenesis including leukocyte adhesion and transmigration into the sub-endothelial space (26). Tools that measure blood flow and characterize regions of disturbed flow can be used to identify vascular locations prone to atherosclerosis, as the connection between atherosclerotic plaque localization and regions of disturbed blood flow has been repeatedly demonstrated.

2.1.2. Atherosclerosis—As atherosclerosis progresses, fatty plaques develop that partially occlude the vessel immediately downstream of the lesion. This flow disturbance reduces the wall shear stress, inducing endothelium-dependent vascular remodeling consisting of intima-media thickening and reduced vessel diameter (27). The development of fatty plaques and intima-media thickening also alters the mechanical properties of blood vessels, resulting in increased cardiovascular morbidity and mortality risk. Additionally, plaques in regions of low wall shear stress progress to have more necrotic cores and fibrous tissue, suggesting an increased risk of plaque rupture (28). Measurement tools that enable the quantification of the physical properties of blood vessels and blood flow have been developed in order to provide information on the risk and progression of atherosclerosis.

2.2. Measurement Tools

Tools that measure the physical properties of blood vessels and blood flow have been employed to study and monitor the progression of vascular pathologies. In addition, mathematical models have been developed to predict the physical parameters of the vasculature, such as wall shear stresses and micro pressures, which would otherwise be difficult to acquire experimentally *in vitro* or *in vivo* (29). When combined with powerful numerical techniques, such as finite element analysis (FEA), these mathematical models have been employed to improve, for instance, the assessment for the risk of rupture of an abdominal aortic aneurysm (AAA) (30). These tools and models will be reviewed in more depth below.

2.2.1. Angiography—Angiography of the blood vessels is routinely performed to identify areas of stenosis, narrowing or blockages of normal blood flow (31). This procedure relies on the insertion of a catheter into the femoral artery or vein for investigation of the arterial or venous system, respectively. The catheter is then used for delivery of a radio-opaque contrast agent that rapidly mixes with blood at the injection site. At the time of contrast

injection, a series of X-rays of the relevant location is performed to capture both still frames and movies for the measurement of lumen diameter and blood flow through the vessels. In the peripheral cardiovascular system, digital subtraction angiography is often employed where a background X-ray of the bones and tissue at the injection site is subtracted from the total X-ray image, giving an image of the contrast alone (32). Digital subtraction angiography requires the acquisition of images at a rate of 2–3 frames per second for the quantification of blood flow through the vessels, and is limited to detection of the lumen of the vessels, albeit with good spatial resolution (0.3–0.4 mm); yet, angiography cannot provide information about vessel wall thickness or tissue structure.

2.2.2. Ultrasound Imaging—Diagnostic external ultrasound imaging is one of the non-invasive measurement tools for the investigation of blood vessel diameter and wall thickness. Doppler ultrasound allows for the measurement of the physical parameters of blood flow including blood flow rate, areas of disturbed flow, and valvular regurgitation (33). Intravascular ultrasound employs the same general technique as utilized by external ultrasound whereby a miniature transducer is located at the end of a catheter to produce images of vessel structure from within the cardiovascular system, eliminating scatter by other tissues and depth penetration issues. The spatial resolution of intravascular ultrasound (using a standard 20 to 40 MHz transducer) is 100 μm axially, and 200–250 μm laterally (34). Intravascular ultrasound provides information about vessel narrowing, plaque size and composition, as well as valve functionality (35).

2.2.3. Contrast Enhanced Ultrasound—The coupled use of microbubbles with ultrasound allows for non-invasive imaging of the cardiovascular system (36). Microbubbles consist of a shell composed of proteins, lipids, or polymers and a gas core consisting of air, nitrogen, or heavy gas such as perfluorocarbons. The microbubbles compress and oscillate when exposed to an ultrasound frequency field in a manner unique from the surrounding blood and tissue which allows for a strong signal in the vessel lumen. Microbubbles are especially useful when investigating blood flow in small diameter vessels including capillary beds, and allows for the extension of Doppler-based techniques below the lower limit of blood flow (<1cm/sec). Additionally, microbubbles are being investigated for their therapeutic use in the molecular imaging of thrombus formation (37) and thrombolysis (38). Microbubbles can be targeted to a clot, where they can be burst by applying a short exposure to high-power ultrasound; the force of the bursting bubbles can break up the clot and help resume flow within the vessel (39).

2.2.4. Optical Coherence Tomography (OCT)—OCT is an echo-based imaging modality that measures light using low coherence interferometry (40). This imaging modality is a high resolution (2–20 μm), high speed (1ns to as fast as 30 fs for 10 μm resolution), non-invasive tomographic imaging technique that allows 3D imaging of the cardiovascular system in animal model systems with transparent tissue such as tadpoles, zebrafish, mouse and embryonic chick hearts (41). OCT allows the measurement of both blood flow and velocity, with exquisite spatial and temporal resolution, making it an ideal imaging modality for the study of heart development in embryonic hearts (42). OCT imaging of the human vasculature is limited to the utility of intravascular OCT, where an OCT core is located at the distal tip of a catheter. As red blood cells scatter the OCT signal, blood needs to be temporarily cleared by an injection of x-ray contrast medium throughout the duration of the OCT pullback to give information about the vessel wall microstructure with very fine resolution (~10 μm). Intravascular OCT can provide information about lumen size, wall thickness, plaque size and composition with higher resolution than intravascular ultrasound.

2.2.5 Flow-sensitive 4D-Magnetic Resonance Imaging (4D-MRI—Also known as magnetic resonance velocimetry, flow-sensitive four-dimensional (4D)-MRI allows for analysis of blood flow parameters and measurement of structural blood vessel features, such as vessel diameters (43). Spatial resolution for these volumes are on the order 2 mm^3 with 40 ms scans, allowing for scans of large vessels on the order of 10–20 minutes for detailed flow and volume information. In 4D-MRI, there is no need for optical access, special flow markers, or exogenous contrast enhancing. Blood flow velocities can be measured along single lines, in planes, or in full 3D volumes (albeit with sub-millimeter resolution). Higher order flow patterns such as helical flow or vortex can also be imaged and analyzed. Data analysis is required for reduction of background noise, antialiasing, and eddy current correction. After analysis, vectorial wall shear stress and oscillatory shear index can be calculated.

2.2.6.1 Bright Field Microscopy—The use of optical microscopy is ubiquitous in the investigation of cellular organisms. One powerful tool available to vascular biologists that takes advantage of multiple microscopy techniques is *ex vivo* isolated vessel preparation (44).

In this technique, a vessel is dissected away from its resident tissue and cannulated in a bath chamber in order to study blood vessel dynamics. This technique has been used to study vessels in many vascular beds including the brain (45), heart (46), and gut (47) with vessels ranging in size from 12 μm microvessels (47) to 200 μm arteries (45). In addition to having pharmacological access to the intra-luminal space of the blood vessel, there is also semi-restricted access to the extra-luminal space through the bath solution. While one of the strengths of this technique is that it allows the study of vascular reactivity within intact blood vessels, the cell-specific roles of blood vessels can also be teased apart through the selective removal of parts of the blood vessel such as the endothelial lining. Coupled to wide-field bright field microscopy, this technique allows for the non-invasive quantification of dynamic changes in blood vessel diameter with optical calipers in response to various stimuli including changes in pressure, flow, or chemotatic gradients.

2.2.6.2 Fluorescence Microscopy—Fluorescence microscopy is one of the most widely used research tools for modern cell biology. Through the use of highly specific fluorescent labeling techniques such as immunocytochemistry, *in situ* hybridization, or fluorescent protein tags, the spatial distribution and dynamics of proteins, subcellular structures or genomic sequences of interest can be analyzed in chemically fixed or living samples. Furthermore, the advent of fluorescent calcium indicators (48) and membrane potential dyes (49) has made it possible to utilize fluorescent microscopy techniques to study questions that once were only measureable though electrophysiology. Moreover, these fluorescent indicators are less invasive than electrophysiology techniques and allow for greater spatial resolution. Paired with genetically engineered animals that have tissue-specific fluorescent reporters, co-localization analysis can provide cell-specific identification of labeling events (50).

2.2.7. Mathematical Modeling and Abdominal Aortic Aneurysms—Mathematical modeling is an effectual, cost-effective tool that provides investigators with opportunities to: i) explore novel avenues for addressing a research question; ii) build a fundamental understanding of the problem being studied; and iii) narrow knowledge gaps. When applied with numerical methods, such as finite element analysis (FEA), mathematical models provide important insight about a design's competency and stability. In the case of AAAs, for example, FEA and mathematical models are used to compute vascular wall stresses

(forces per unit area). The stresses are subsequently employed to assess the risks of rupture of AAAs (30).

To model and solve an AAA biomechanical problem, a patient's AAA geometry must first be acquired from medical images, such as CT and MRI. This is achieved by using image segmentation algorithms that extract the outer wall and lumen contours from the cross-sectional images. Computationally, the contours are stacked to reconstruct the aneurismal geometry in the form of a mesh, which is subsequently imported to a finite element program. To properly simulate the physical structure and environment of the aneurysm, knowledge of the aortic tissue's material mechanical properties (e.g. tensile and compressive strengths and measures of stiffness), vascular loads, and boundary conditions are indispensable (51). Methods for the acquisition of material properties are discussed further in Section 2.2.8. The intraluminal loads applied to the model walls are the brachial systolic and diastolic blood pressures measured at the time of the initial CT scan is taken. The typical boundaries imposed on the model include fixing the ends of mesh to simulate the connection of the AAA to the surrounding aorta. Once pertinent information is inputted into FEA software, the finite element program numerically solves a complex set of partial differential equations over the intricate AAA continuum by: i) dividing the complex aneurysmal geometry into discrete, smaller domains; and ii) simplifying the partial differential equations into algebraic equations involving a finite number of parameters within the smaller domains. From these computations, important physical measures, such as the extent of a model's deformation in response to the applied loads and the wall stresses, are obtained. One limitation of mathematical models is their sensitivity to the input parameters and set-up. If minimal care is placed in choosing the appropriate boundary conditions, for example, the models will yield incorrect wall stress results or solutions may fail to converge.

2.2.8. Tissue Material Properties and Tensile Testing—Conventionally, the physical parameters used in the modeling of a patient's AAA are not patient-specific; rather, they are derived from tensile testing measurements performed on tissues obtained from a population of cadavers or patients undergoing elective repair (52). For uniaxial tensile testing of aortic tissue, the specimen is secured on brackets that move in opposite directions. As the tissue is stretched, a tension load cell placed on one end of the brackets converts the imposed load into an analog electrical signal. An analog-to-digital device subsequently digitizes the signal. The tension forces and the change in specimen length are recorded throughout the experiment. The tissue is stretched until failure to also acquire the failure tension, which is a good indicator of a tissue's vulnerability. Because the specimen in uniaxial tensile testing is extended in one dimension, knowledge gained about the failure tensions is limited to the tested direction. In contrast, biaxial tensile testing, which measures an AAA tissue's tension forces in the circumferential and longitudinal directions, may provide a more complete assessment of a tissue's wall mechanics and an opportunity for modeling AAA tissue more accurately (53).

2.2.9. Tissue Elasticity Imaging—Employing tensile testing measurements for the acquisition of patient-specific aneurismal material properties is not feasible due to its invasive protocol. Tissue elasticity imaging has been employed to non-invasively determine these material properties for the liver, kidney and heart, but its potential use for the characterization of patient-specific AAA material properties needs further assessment. In static elastography, a more common form of elastographic imaging, a tissue is externally compressed with a transducer and the pre- and post-compression imaging line pair data are subsequently acquired. A cross-correlation analysis is performed on the compression line pair data in order to compute a strain field. The applied stress is assumed to be a function of the ratio of the circular compressor radius and the axial distance between the compressor and the point of interest within the tissue (54). Using the strain and stress, the tissue elastic

modulus, a measure of stiffness, can be calculated. One limitation of elastography is its sensitivity to small motions, which can affect the cross-correlation analysis resulting in a probable erroneous strain field. Addressing the limitations in system stability can aid in improving elastography as a medical application. If elastography can be employed to assess AAA patient-specific properties, the acquired information may be instrumental in not only evaluating the strength of a patient's AAA but also in improving the accuracy of wall stress computations and the assessment of aneurismal rupture risk.

3. Blood Cell Physiology and Measurement Tools

3.1. Introduction and Background

Blood is an essential constituent of the circulatory system and is responsible for body temperature control, coagulation, pH regulation, oxygen and nutrient distribution to tissues, and removal of waste products from tissues. Blood is primarily composed of blood cells suspended in an aqueous solution of plasma. The three main types of blood cells are red blood cells (RBCs), white blood cells and platelets. Plasma is composed of water, plasma proteins, dissolved nutrients, and waste products. The average adult blood volume is about 5 L and has an average density of 1060 kg/m^3 (55).

3.1.1. Red Blood Cells—As the most abundant cell type in the blood, red blood cells (RBCs), or erythrocytes, compose approximately 99% of all blood cells at a concentration of 4.7 to 6.1 million cells/μL in humans (56). They are produced daily at a rate of 2.56×10^9 cells/kg, and have a life span of about 120 days in the circulation. RBCs play a critical role transporting oxygen from the lungs to other tissues in the body via the circulatory system. RBCs utilize hemoglobin to fix and transport oxygen and carbon dioxide in the blood. An individual molecule of hemoglobin can bind up to four molecules of oxygen and effectively transport 97% of the available oxygen to tissues (57). Hemoglobin is also responsible for the red color of erythrocytes, yielding light absorption peaks at the 275nm and 417nm wavelengths (58).

Human RBCs are anucleated cells that possess a biconcave disk shape with a diameter of 5.5 to 8.8 μm and a thickness of 2 μm at the periphery and 1 μm at the narrowest point (center). Their surface area is approximately 120 μm^2 and their volume is approximately 85 to 90 μm^3. They have a cytoskeletal structure formed by spectrin, a flexible rod-like molecule that maintains its shape, and a membrane that is composed of 40% lipid bilayer, 52% proteins, and 8% carbohydrates. Some of the most important physical features of RBCs are their high elasticity and deformability. The elastic shear modulus for RBCs at 25°C is approximately 6.8 μN/m, as measured by micropipette aspiration, while the membrane shear modulus is approximately 20 μN/m, and the area compressibility modulus is approximately 7.5 ± 2.5 μN/m. The physical parameters of RBCs allow them to circulate through the reticuloendothelial system through capillaries as small as 3 μm in diameter.

Several pathological disorders are associated with alterations in the physical parameters of RBCs. In the case of sickle cell anemia, mutations in hemoglobin result in the polymerization of hemoglobin S and subsquent distortion of the RBC morphology, including increasing the effective shear modulus of RBCs by two to three fold (59). Other hemoglobinopathies include hemoglobin C disease, hemoglobin S-C disease, and various types of thalassemia (60).

3.1.2. White Blood Cells—White blood cells, or leukocytes, which make about 1% of total blood cells, are cells of the immune system that combat infection and defend the body against foreign materials. They are grouped into three major types: granulocytes, monocytes, and lymphocytes. Granulocytes contain densely staining granules in their cytoplasm and are

classified into three types: neutrophils, which make up about 5×10^9 cells/L (61), eosinophils, which comprise about 4×10^7 cells/L (62), and basophils, which make up about 4×10^7 cells/L of human blood (63). Human neutrophils, at a diameter of 10–12 μm, are the most common type of granulocytes, and are produced at a rate of 2×10^{11} cells per day. They transit in the blood for approximately 5 to 7 days, during which time they constantly survey for microorganisms such as bacteria. Neutrophils target and destroy pathogens by a process termed phagocytosis, whereby bacteria are engulfed and trafficked to intracellular vesicles, where they are destroyed using degradative enzymes stored in cytoplasmic granules. As a result, neutrophils play a key role in the host innate immunity against bacterial infection. Basophils, which are 12–15 μm in diameter and eosinophils, which are 10–12 μm in diameter, are both involved in allergic inflammatory reactions. Basophils secrete histamine to help mediate inflammatory reactions, while eosinophils destroy parasites and modulate allergic inflammatory responses (64). Monocytes, which are 7–9 μm in diameter and present in the blood at a concentration of 4×10^8 cells/L (65), mature into macrophages upon leaving the bloodstream, and share the responsibility with neutrophils of being the main phagocytic members in the body (66). In addition, during their 25 hr transit in the blood, monocytes also replenish the body's supply of dendritic cells, which specialize in presenting antigens to lymphocytes to trigger an adaptive immune response. Lymphocytes, which transit in blood for approximately 200 days, are divided into two classes that are both involved in immune responses: B-cells, which are primarily responsible for making antibodies, and T-cells, which kill virus-infected cells and regulate other leukocyte activities. B-cells circulate at a level of 2×10^9 cell/L of blood and are 7–8 μm in diameter, while T-cells circulate at a concentration of 1×10^9 cells/L of blood and are 12–15 μm in diameter (67).

Several pathologies are associated with perturbations in the physical parameters of these white blood cell populations. For instance, a reduction in the number of white blood cells, in particular neutrophils, results in leukopenia and renders individuals at higher risk for infection. In contrast, in leukemia, an abnormal increase in immature white blood cells is associated with cancer of the blood or bone marrow (24). Other diseases that develop due to aberrant quantities of leukocytes include lymphoma, which results from an overproduction of B and T lymphocytes, and myeloma, which results from an abnormal accumulation of plasma B cells in the bone marrow (68).

3.1.3. Platelets—Platelets, or thrombocytes, are the smallest cells in the blood, with a diameter of 2 to 4 μm, a thickness of 70 to 90 Å, and a density of 1.04 to 1.08 g/mL. With a lifespan of about 5 to 9 days in humans, these cells are present in the blood at a concentration of 150 to 350 billion cells/L, and are produced by megakaryocytes at a rate of 10^{11} platelets per day (69). Platelets play a critical role in maintaining hemostasis by adhering to the lining of blood vessels upon endothelial cell injury to initiate thrombus formation (70, 71).

Platelets are anuclear, yet possess other common cellular structures such as microtubules, alpha and dense granules, mitochondria, Golgi, and lysosomes. Platelets exhibit an open canalicular system, which is a dense tubular system that plays an essential role in the rapid transport of agonists and platelet releasate to and from the cell, respectively (72). The outer glycocalyx membrane of platelets is key for the assembly of different enzyme complexes that culminate in coagulation, while the interior membrane is covered by cross-linked actin (73). Platelets are refractile, and their elastic moduli ranges from 1 and 50 kPa (74). When spread, platelet stiffness has been measured as between 1.5 to 4 kPa in the pseudonucleus, 4 kPa in the inner web, and 10 to 40 kPa in the outer web.

Several severe pathological conditions are associated with changes in the physical parameters of platelets (75). For instance, conditions such as thrombocytopenia are associated with a dramatic drop in platelet count below 50,000cells/μL, which results in an impaired ability of patients to maintain hemostasis (76). Other conditions that are associated with altered platelet function are disseminated intravascular coagulation, myelodysplasia, Scott's Syndrome, Storage Pool disorder, Bernard Soulier Syndrome, Glanzmann's Thrombaesthenia, hemolytic anemia, hypersplendis, thrombocytosis, chronicmyelogenous leukemia, and polycythemia vera (77).

3.1.3. Plasma—Blood plasma is a light yellow, semi-transparent, aqueous solution in which blood cells are suspended. Plasma constitutes approximately 55% of the blood volume, with blood cells constituting the remaining 45%. The main components of plasma are water (90%), protein (8%), inorganic salts (0.9%), and organic substances (1.1%) (78). Proteins in the plasma such as prothrombin, fibrinogen and other coagulation factors are essential to facilitate the coagulation cascade (79), while proteins such as albumin are critical in maintaining the osmotic pressure of blood (80).

A number of clinical disorders are associated with deficiencies in blood plasma components, and can be treated following infusion of missing coagulation factors. For instance, infusion of the plasma protein Factor VIII or IX is the main treatment for FVIII- or FIX-deficient patients (hemophilia A or B), respectively (81). Other treatments using plasma include immunoglobulin treatment for patients with antibody deficiencies or antithrombin concentrates used for patients with antithrombin deficiencies. Albumin has also been used to treat acute hypolemia (e.g. surgical blood loss, trauma, hemorrhage) as well as chronic liver disease (82).

3.2. Measurement Tools

Numerous measurement systems have been developed to analyze properties of blood cells, plasma, and blood disorders and disease. A few common techniques to measure the physical parameters of blood cells and components include atomic force microscopy (AFM), flow cytometry, microfluidics, micropipette aspiration, optical microscopy, optical tweezers, and electron microscopy (83).

3.2.1. Atomic Force Microscopy (AFM—AFM is a useful method to measure the mechanical properties of living cells, and has been widely utilized to characterize the physical properties of blood cells (84). Invented in 1986, contact AFM uses a soft cantilever probe that applies a known force or stress to a cell, and measures the deformation in order to determine the cell elastic properties (e.g., spring constant and Young's modulus) (85). The contact AFM probe typically depresses the cell surface at a constant velocity, resulting in the application of an increasing force. Contact AFM is capable of measuring forces down to 5–10 pN with a spatial resolution on the nanometer scale. Scanning AFM, which emerged a few years after contact AFM, uses a single frequency to excite the probe while being scanned across a sample to generate a three-dimensional topographical surface profile to investigate cell biophysical parameters (e.g., thickness, width, surface area, and volume). Multifrequency AFM is a new and promising technique that improves the spatial and time resolution of traditional AFM and can measure subsurface properties through the use of multiple frequencies of the probe's oscillation (86)

3.2.2. Flow Cytometry—Flow cytometry is a non-destructive tool useful for quantifying phenotypes and sorting sizes of blood cell samples (e.g., cells, microorganisms, chromosomes and cell organelles). Flow cytometry accomplishes sorting by passing a flow stream of suspended particles single-file through a measurement station where they are

illuminated by a light source. The light is scattered when it hits a particle, and analysis of the angle of scattering can reveal sample parameters (e.g., size, shape, viability, volume and density) (87). These measurements rely on the fact that a linear response in light scattering to diameter is observed over a wide range of particle sizes. Moreover, light scattering can also strongly depend on particle structure (e.g., absorbency of material, surface texture, and internal granularity), allowing for the characterization of the internal structure of cells or quantification of cell-cell interactions (88). Furthermore, flow cytometry can be used to detect fluorescent signals for the characterization of biological samples (88). Fluorescent labeling of cell surface or intracellular molecules allows for both the detection and selection of cell populations for cell sorting.

Fluorescence-activated cell sorting is a specialized flow cytometry technique that sorts heterogeneous mixtures of cells according to subtype or epitope expression based on light scattering and fluorescent characteristics. Flow cytometry-based analysis has been extensively employed to characterize the physical parameters of RBCs, white blood cells, and platelets (89).

3.2.3. Microfluidics—The study of thrombus formation *ex vivo* can occur in closed or open systems, with or without flow (90). Microfluidic devices, which constrain fluids to a small (typically submillimeter) scale, facilitate characterization of platelet function, coagulation biology, cellular biorheology, adhesion dynamics, and pharmacology, under physiologically relevant shear flow conditions. Microfluidic devices have been developed to separate particles through the use of microelectrodes or asymmetric obstacles. The advantages of microfluidics include lower cost and complexity than flow cytometry and the ability to measure hydrodynamic cell size. Researchers and clinicians have used microfluidic devices to fractionate blood and separate white blood cells, red blood cells and plasma based on geometric parameters. Microfluidics devices are ideal for multicolor imaging of platelets, fibrin, and phosphatidylserine (91), and provide a human blood analog to mouse injury models (92). Overall, microfluidic advances offer many opportunities for research, drug testing under relevant hemodynamic conditions, and clinical diagnostics.

3.2.4. Micropipette Aspiration—Micropipette aspiration (micropipette suction) is a measurement tool capable of characterizing the mechanical properties of blood cells. With this technique, the surface of a cell is aspirated into a pipette with a known suction pressure and the extension of the edge of the cell into the pipette or the movement of the cell away from an attachment point is measured (93). Subsequent modeling and interpretation of these measurements can be used to determine the elastic and viscous properties of cells. Capable of pressures in the range of 0.1 $pN/\mu m^2$ to atmospheric pressure, and forces from 10 pN to 10^4 nN, micropipette experiments have been utilized to characterize the mechanical properties of both soft cells (e.g., red blood cells and neutrophils) and rigid cells (e.g., endothelial cells and chondrocytes).

3.2.5. Optical Microscopy—Optical (light) microscopy has been the key tool used by researchers for visualizing and studying blood cells, blood disorders and disease. Classical optical microscopy involves passing transmitted or reflected light from a sample through a lens or series of lenses to magnify the sample for visualization (94). However, many biological samples are thin or have high reflectivity, which results in poor contrast or reduced visibility. This shortcoming has lead to development of imaging modalities (e.g., polarized light, differential interference contrast, fluorescence illumination, phase contrast imaging, and darkfield illumination) that increase contrast or color variations to improve sample visualization (95). Further, the combination of ultraviolet microscopy and microspectroscopy has been used to quantify hemoglobin concentration in red blood cells through analysis of light absorption at different wavelengths (96). Other studies have used

phase retrieval methods applied to phase contrast microscopy to investigate volume, mass and density of RBCs (97) and platelet aggregates (98, 99). Diffraction phase microscopy is another technique that utilizes principles of optical interferometric imaging combined with mathematical modeling to obtain cell mechanical parameters (e.g., spring constant, bending modulus and area modulus) (100). Diffraction phase microscopy has previously been applied to quantify thermal fluctuations of red blood cell membranes and to identify mechanical changes of red blood cells as they transform from a healthy shape to an abnormal, unhealthy shape.

3.2.6. Optical Tweezers—Mechanical properties of blood cells can also be studied using optical tweezers (laser tweezers). Optical tweezers use the intrinsic property of light to exert forces on matter to trap a bead within a beam of light. This small bead suspended in the optical trap can be adhered to a cell surface. Movement of the cell away from the bead will result in the pulling of the cell membrane. The force of extension of the cell membrane can be measured using the deflection of the bead in the optical trap perpendicular to the optical axis. Effects of Brownian motion and thermal forces cannot be avoided with optical tweezers, however, resulting in a force measurement limit of about 50 pN depending on the system. Optical tweezers represent a powerful tool for studying blood cell rheology and receptor-binding kinetics (101).

3.2.7 Electron Microscopy—Transmission electron microscopy (TEM) is achieved by passing a beam of electrons through the sample. Transmitted electrons are focused onto a high-resolution photographic plate to create a two-dimensional image. Scanning electron microscopy (SEM), the reflection mode analog to TEM, uses backscattered electrons to reveal surface details of the sample. TEM enables imaging of samples with a magnification up to 50 million times and a resolution of 0.5 angstroms, while SEM is capable of a magnification of 2 million times and a resolution of 0.4 nm. TEM and SEM have been instrumental in visualizing the cellular constituents of blood in healthy and disease states (102). The combination of immunolabeling with TEM and/or SEM provides insight into the interaction of biomolecules within and on the surface of blood cells in normal or pathological states (103).

Three-dimensional EM imaging of blood cells has only recently been possible through the use of focused ion beam (FIB) ablation in conjunction with SEM. In FIB-SEM, a sample plane is first imaged with SEM and then that plane is removed through FIB ablation to reveal a deeper surface in the specimen. FIB-SEM has an axial resolution of 4.5 nm and a transverse resolution of 0.8 nm and currently requires tens of hours to complete image acquisition. This technology has been applied to the investigation of myosin IIA mediated organelle distribution in megakaryocytes and platelets (104). Although currently expensive and time consuming, the guiding technological principles behind FIB-SEM promise to enhance our knowledge of blood cell ultrastructure and ultimately guide our future multi-scale understanding of blood cell function.

Concluding Remarks

The development of measurement tools with resolution from the nanometer to centimeter length scales has allowed for the study of the physical parameters of the circulatory system. Together, these techniques provide a platform for the development of novel biomedical approaches for the detection, diagnosis and treatment of cardiovascular diseases.

Acknowledgments

We are grateful to Juliana Porter for technical assistance. This work was supported by the National Institutes of Health (NIH) grants U54CA143906 and R01HL101972 to O.J.T.M, R01HL095474 and R01HL103728 to M.T.H., R01HL101972-S1 to F.A.C, T32HL094294 to J.W.N., 5T32HL094294 to C.M.J., TL1TR000129 to J.Z., and the National Science Foundation (NSF) grants DGE-0925180 to J.J.G. D.C.P. is supported by an OHSU Graduate Research Fellowship and NIH grant HL093056. W.Y.L. is supported by NIH grant R01NS071116. J.Z. is supported by NSF grant DBI-1052688. S.M.B. is a Whitaker International Fellow. O.J.T.M. is an American Heart Association Established Investigator (13EIA12630000). W.Y.L. and J.J.G are ARCS Scholars.

Abbreviations

AAA	abdominal aortic aneurysm
AFM	atomic force microscopy
CT	computed tomography
EC	endothelial cell
ECG	electrocardiogram
FEA	finite element analysis
MI	myocardial infarction
MRI	magnetic resonance imaging
OCT	optical coherence tomography
PET	positron emission tomography
RBC	red blood cell
SEM	scanning electron microscopy
TEM	transmission electron microscopy
US	ultrasound

References

1. Gittenberger-de Groot AC, Winter EM, Bartelings MM, Goumans MJ, DeRuiter MC, Poelmann RE. The arterial and cardiac epicardium in development, disease and repair. Differentiation. 2012 Jul; 84(1):41–53. [PubMed: 22652098]
2. Kimura K, Ieda M, Fukuda K. Development, maturation, and transdifferentiation of cardiac sympathetic nerves. Circ Res. 2012 Jan 20; 110(2):325–336. [PubMed: 22267838]
3. Simon MA. Assessment and treatment of right ventricular failure. Nat Rev Cardiol. 2013 Apr; 10(4):204–218. [PubMed: 23399974]
4. Rodeheffer RJ, Gerstenblith G, Becker LC, Fleg JL, Weisfeldt ML, Lakatta EG. Exercise cardiac output is maintained with advancing age in healthy human subjects: cardiac dilatation and increased stroke volume compensate for a diminished heart rate. Circulation. 1984 Feb; 69(2):203–213. [PubMed: 6690093]
5. Fraccarollo D, Galuppo P, Bauersachs J. Novel therapeutic approaches to post-infarction remodelling. Cardiovasc Res. 2012 May 1; 94(2):293–303. [PubMed: 22387461]
6. Motwani M, Jogiya R, Kozerke S, Greenwood JP, Plein S. Advanced cardiovascular magnetic resonance myocardial perfusion imaging: high-spatial resolution versus 3-dimensional whole-heart coverage. Circ Cardiovasc Imaging. 2013 Mar 1; 6(2):339–348. [PubMed: 23512780]
7. Drew BJ, Califf RM, Funk M, Kaufman ES, Krucoff MW, Laks MM, et al. Practice standards for electrocardiographic monitoring in hospital settings: an American Heart Association scientific statement from the Councils on Cardiovascular Nursing, Clinical Cardiology, and Cardiovascular Disease in the Young: endorsed by the International Society of Computerized Electrocardiology and

the American Association of Critical-Care Nurses. Circulation. 2004 Oct 26; 110(17):2721–2746. [PubMed: 15505110]

8. Windecker S, Bax JJ, Myat A, Stone GW, Marber MS. Future treatment strategies in ST-segment elevation myocardial infarction. Lancet. 2013 Aug 17; 382(9892):644–657. [PubMed: 23953388]
9. Daniel WG, Mugge A. Transesophageal echocardiography. N Engl J Med. 1995 May 11; 332(19): 1268–1279. [PubMed: 7708072]
10. Schuleri KH, George RT, Lardo AC. Applications of cardiac multidetector CT beyond coronary angiography. Nat Rev Cardiol. 2009 Nov; 6(11):699–710. [PubMed: 19851349]
11. Catana C, Guimaraes AR, Rosen BR. PET and MR imaging: the odd couple or a match made in heaven? J Nucl Med. 2013 May; 54(5):815–824. [PubMed: 23492887]
12. Greco A, Fiumara G, Gargiulo S, Gramanzini M, Brunetti A, Cuocolo A. High-resolution positron emission tomography/computed tomography imaging of the mouse heart. Exp Physiol. 2013 Mar; 98(3):645–651. [PubMed: 23118016]
13. Johnson SG, Peters S. Advances in pharmacologic stress agents: focus on regadenoson. J Nucl Med Technol. 2010 Sep; 38(3):163–171. [PubMed: 20724531]
14. Lamb HJ, van der Meer RW, de Roos A, Bax JJ. Cardiovascular molecular MR imaging. Eur J Nucl Med Mol Imaging. 2007 Jun; 34(Suppl 1):S99–S104. [PubMed: 17505824]
15. Li X, Rooney WD, Springer CS Jr. A unified magnetic resonance imaging pharmacokinetic theory: intravascular and extracellular contrast reagents. Magn Reson Med. 2005 Dec; 54(6):1351–1359. [PubMed: 16247739]
16. Li X, Springer CS Jr, Jerosch-Herold M. First-pass dynamic contrast-enhanced MRI with extravasating contrast reagent: evidence for human myocardial capillary recruitment in adenosine-induced hyperemia. NMR Biomed. 2009 Feb; 22(2):148–157. [PubMed: 18727151]
17. Tofts PS. Modeling tracer kinetics in dynamic Gd-DTPA MR imaging. J Magn Reson Imaging. 1997 Jan-Feb;7(1):91–101. [PubMed: 9039598]
18. Tofts PS, Brix G, Buckley DL, Evelhoch JL, Henderson E, Knopp MV, et al. Estimating kinetic parameters from dynamic contrast-enhanced T(1)-weighted MRI of a diffusable tracer: standardized quantities and symbols. J Magn Reson Imaging. 1999 Sep; 10(3):223–332. [PubMed: 10508281]
19. Nacif MS, Zavodni A, Kawel N, Choi EY, Lima JA, Bluemke DA. Cardiac magnetic resonance imaging and its electrocardiographs (ECG): tips and tricks. Int J Cardiovasc Imaging. 2012 Aug; 28(6):1465–1475. [PubMed: 22033762]
20. Sumpio BE, Riley JT, Dardik A. Cells in focus: endothelial cell. Int J Biochem Cell Biol. 2002 Dec; 34(12):1508–1512. [PubMed: 12379270]
21. Busse R, Fleming I. Vascular endothelium and blood flow. Handb Exp Pharmacol. 2006; (176 Pt 2):43–78. [PubMed: 16999224]
22. Vartanian KB, Berny MA, McCarty OJ, Hanson SR, Hinds MT. Cytoskeletal structure regulates endothelial cell immunogenicity independent of fluid shear stress. Am J Physiol Cell Physiol. 2010 Feb; 298(2):C333–C341. [PubMed: 19923423]
23. Vartanian KB, Kirkpatrick SJ, McCarty OJ, Vu TQ, Hanson SR, Hinds MT. Distinct extracellular matrix microenvironments of progenitor and carotid endothelial cells. J Biomed Mater Res A. 2009 Nov; 91(2):528–539. [PubMed: 18985765]
24. Cines DB, Pollak ES, Buck CA, Loscalzo J, Zimmerman GA, McEver RP, et al. Endothelial cells in physiology and in the pathophysiology of vascular disorders. Blood. 1998 May 15; 91(10): 3527–3561. [PubMed: 9572988]
25. Anderson DE, Hinds MT. Extracellular matrix production and regulation in micropatterned endothelial cells. Biochem Biophys Res Commun. 2012 Oct 12; 427(1):159–164. [PubMed: 22995321]
26. Zilversmit DB. Atherogenesis: a postprandial phenomenon. Circulation. 1979 Sep; 60(3):473–485. [PubMed: 222498]
27. Berliner JA, Navab M, Fogelman AM, Frank JS, Demer LL, Edwards PA, et al. Atherosclerosis: basic mechanisms. Oxidation, inflammation, and genetics. Circulation. 1995 May 1; 91(9):2488–2496. [PubMed: 7729036]

28. van der Wal AC, Becker AE, van der Loos CM, Das PK. Site of intimal rupture or erosion of thrombosed coronary atherosclerotic plaques is characterized by an inflammatory process irrespective of the dominant plaque morphology. Circulation. 1994 Jan; 89(1):36–44. [PubMed: 8281670]
29. Gijsen F, van der Giessen A, van der Steen A, Wentzel J. Shear stress and advanced atherosclerosis in human coronary arteries. J Biomech. 2013 Jan 18; 46(2):240–247. [PubMed: 23261245]
30. Venkatasubramaniam AK, Fagan MJ, Mehta T, Mylankal KJ, Ray B, Kuhan G, et al. A comparative study of aortic wall stress using finite element analysis for ruptured and non-ruptured abdominal aortic aneurysms. Eur J Vasc Endovasc Surg. 2004 Aug; 28(2):168–176. [PubMed: 15234698]
31. Berger SA, Jou LD. Flows in Stenotic Vessels. Annual Review of Fluid Mechanics. 2000; 32(1): 347–382.
32. Lu L, Zhang LJ, Poon CS, Wu SY, Zhou CS, Luo S, et al. Digital subtraction CT angiography for detection of intracranial aneurysms: comparison with three-dimensional digital subtraction angiography. Radiology. 2012 Feb; 262(2):605–612. [PubMed: 22143927]
33. Otto CM, Pearlman AS, Comess KA, Reamer RP, Janko CL, Huntsman LL. Determination of the stenotic aortic valve area in adults using Doppler echocardiography. J Am Coll Cardiol. 1986 Mar; 7(3):509–517. [PubMed: 3950230]
34. Mintz GS, Nissen SE, Anderson WD, Bailey SR, Erbel R, Fitzgerald PJ, et al. American College of Cardiology Clinical Expert Consensus Document on Standards for Acquisition, Measurement and Reporting of Intravascular Ultrasound Studies (IVUS). A report of the American College of Cardiology Task Force on Clinical Expert Consensus Documents. J Am Coll Cardiol. 2001 Apr; 37(5):1478–1492. [PubMed: 11300468]
35. Park SJ, Ahn JM, Kang SJ. Unprotected left main percutaneous coronary intervention: integrated use of fractional flow reserve and intravascular ultrasound. J Am Heart Assoc. 2012 Dec. 1(6):e004556. [PubMed: 23316329]
36. Wrenn SP, Dicker SM, Small EF, Dan NR, Mleczko M, Schmitz G, et al. Bursting bubbles and bilayers. Theranostics. 2012; 2(12):1140–1159. [PubMed: 23382772]
37. McCarty OJ, Conley RB, Shentu W, Tormoen GW, Zha D, Xie A, et al. Molecular imaging of activated von Willebrand factor to detect high-risk atherosclerotic phenotype. JACC Cardiovasc Imaging. 2010 Sep; 3(9):947–955. [PubMed: 20846630]
38. Kiessling F, Fokong S, Koczera P, Lederle W, Lammers T. Ultrasound microbubbles for molecular diagnosis, therapy, and theranostics. J Nucl Med. 2012 Mar; 53(3):345–348. [PubMed: 22393225]
39. Lindner JR, Sinusas A. Molecular imaging in cardiovascular disease: Which methods, which diseases? J Nucl Cardiol. 2013 Oct 4.
40. Subhash HM, Xie H, Smith JW, McCarty OJ. Optical detection of indocyanine green encapsulated biocompatible poly (lactic-co-glycolic) acid nanoparticles with photothermal optical coherence tomography. Opt Lett. 2012 Mar 1; 37(5):981–983. [PubMed: 22378459]
41. Yelin R, Yelin D, Oh WY, Yun SH, Boudoux C, Vakoc BJ, et al. Multimodality optical imaging of embryonic heart microstructure. J Biomed Opt. 2007 Nov-Dec;12(6):064021. [PubMed: 18163837]
42. Shi L, Goenezen S, Haller S, Hinds MT, Thornburg KL, Rugonyi S. Alterations in pulse wave propagation reflect the degree of outflow tract banding in HH18 chicken embryos. Am J Physiol Heart Circ Physiol. 2013 Aug 1; 305(3):H386–H396. [PubMed: 23709601]
43. Markl M, Kilner PJ, Ebbers T. Comprehensive 4D velocity mapping of the heart and great vessels by cardiovascular magnetic resonance. J Cardiovasc Magn Reson. 2011; 13:7. [PubMed: 21235751]
44. Halpern W, Kelley M. In vitro methodology for resistance arteries. Blood Vessels. 1991; 28(1–3): 245–251. [PubMed: 1825797]
45. Golding EM, Robertson CS, Bryan RM Jr. Comparison of the myogenic response in rat cerebral arteries of different calibers. Brain Res. 1998 Mar 2; 785(2):293–298. [PubMed: 9518656]
46. Kuo L, Davis MJ, Chilian WM. Myogenic activity in isolated subepicardial and subendocardial coronary arterioles. Am J Physiol. 1988 Dec; 255(6 Pt 2):H1558–H1562. [PubMed: 2462367]

47. Duling BR, Gore RW, Dacey RG Jr, Damon DN. Methods for isolation, cannulation, and in vitro study of single microvessels. Am J Physiol. 1981 Jul; 241(1):H108–H116. [PubMed: 7195654]
48. Adams SR. How calcium indicators work. Cold Spring Harb Protoc. 2010 Mar.2010(3) pdb top70.
49. Adams DS, Levin M. General principles for measuring resting membrane potential and ion concentration using fluorescent bioelectricity reporters. Cold Spring Harb Protoc. 2012 Apr; 2012(4):385–397. [PubMed: 22474653]
50. Homma R, Baker BJ, Jin L, Garaschuk O, Konnerth A, Cohen LB, et al. Wide-field and two-photon imaging of brain activity with voltage- and calcium-sensitive dyes. Methods Mol Biol. 2009; 489:43–79. [PubMed: 18839087]
51. Vorp DA. Biomechanics of abdominal aortic aneurysm. J Biomech. 2007; 40(9):1887–1902. [PubMed: 17254589]
52. Henebiens M, Vahl A, Koelemay MJ. Elective surgery of abdominal aortic aneurysms in octogenarians: a systematic review. J Vasc Surg. 2008 Mar; 47(3):676–681. [PubMed: 18207352]
53. Volokh KY. Comparison of biomechanical failure criteria for abdominal aortic aneurysm. J Biomech. 2010 Jul 20; 43(10):2032–2034. [PubMed: 20381050]
54. Ophir J, Moriya T, Yazdi Y. A single transducer transaxial compression technique for the estimation of sound speed in biological tissues. Ultrason Imaging. 1991 Jul; 13(3):269–279. [PubMed: 1957424]
55. Wagner DD, Frenette PS. The vessel wall and its interactions. Blood. 2008 Jun 1; 111(11):5271–5281. [PubMed: 18502843]
56. Dzierzak E, Philipsen S. Erythropoiesis: development and differentiation. Cold Spring Harb Perspect Med. 2013 Apr.3(4):a011601. [PubMed: 23545573]
57. Marks PA, Kovach JS. Development of mammalian erythroid cells. Curr Top Dev Biol. 1966; 1:213–252. [PubMed: 4944303]
58. Rubinstein DL, Ravikovich HM. Absorption spectrum of haemoglobin in red cells. Nature. 1946 Dec 28.158(4026):952. [PubMed: 20277889]
59. Poillon WN, Kim BC, Castro O. Intracellular hemoglobin S polymerization and the clinical severity of sickle cell anemia. Blood. 1998 Mar 1; 91(5):1777–1783. [PubMed: 9473246]
60. Thom CS, Dickson CF, Gell DA, Weiss MJ. Hemoglobin variants: biochemical properties and clinical correlates. Cold Spring Harb Perspect Med. 2013 Mar.3(3):a011858. [PubMed: 23388674]
61. Mocsai A. Diverse novel functions of neutrophils in immunity, inflammation, and beyond. J Exp Med. 2013 Jul 1; 210(7):1283–1299. [PubMed: 23825232]
62. Fulkerson PC, Rothenberg ME. Targeting eosinophils in allergy, inflammation and beyond. Nat Rev Drug Discov. 2013 Feb; 12(2):117–129. [PubMed: 23334207]
63. Voehringer D. Protective and pathological roles of mast cells and basophils. Nat Rev Immunol. 2013 May; 13(5):362–375. [PubMed: 23558889]
64. McCarty OJ, Tien N, Bochner BS, Konstantopoulos K. Exogenous eosinophil activation converts PSGL-1-dependent binding to CD18-dependent stable adhesion to platelets in shear flow. Am J Physiol Cell Physiol. 2003 May; 284(5):C1223–C1234. [PubMed: 12529243]
65. Ahn KC, Jun AJ, Pawar P, Jadhav S, Napier S, McCarty OJ, et al. Preferential binding of platelets to monocytes over neutrophils under flow. Biochem Biophys Res Commun. 2005 Apr 1; 329(1): 345–355. [PubMed: 15721313]
66. Pardali E, Waltenberger J. Monocyte function and trafficking in cardiovascular disease. Thromb Haemost. 2012 Nov; 108(5):804–811. [PubMed: 22918193]
67. Litman GW, Rast JP, Fugmann SD. The origins of vertebrate adaptive immunity. Nat Rev Immunol. 2010 Aug; 10(8):543–553. [PubMed: 20651744]
68. Younes A. Beyond chemotherapy: new agents for targeted treatment of lymphoma. Nat Rev Clin Oncol. 2011 Feb; 8(2):85–96. [PubMed: 21151205]
69. Machlus KR, Italiano JE Jr. The incredible journey: From megakaryocyte development to platelet formation. J Cell Biol. 2013 Jun 10; 201(6):785–796. [PubMed: 23751492]
70. Aslan JE, Itakura A, Gertz JM, McCarty OJ. Platelet shape change and spreading. Methods Mol Biol. 2012; 788:91–100. [PubMed: 22130702]

71. Watson SP, Auger JM, McCarty OJ, Pearce AC. GPVI and integrin alphaIIbbeta3 signaling in platelets. J Thromb Haemost. 2005 Aug; 3(8):1752–1762. [PubMed: 16102042]
72. Fox JE. Cytoskeletal proteins and platelet signaling. Thromb Haemost. 2001 Jul; 86(1):198–213. [PubMed: 11487008]
73. Aslan JE, McCarty OJ. Rho GTPases in platelet function. J Thromb Haemost. 2013 Jan; 11(1):35–46. [PubMed: 23121917]
74. Carr ME Jr. Development of platelet contractile force as a research and clinical measure of platelet function. Cell Biochem Biophys. 2003; 38(1):55–78. [PubMed: 12663942]
75. Heemskerk JW, Bevers EM, Lindhout T. Platelet activation and blood coagulation. Thromb Haemost. 2002 Aug; 88(2):186–193. [PubMed: 12195687]
76. Tucker EI, Marzec UM, Berny MA, Hurst S, Bunting S, McCarty OJ, et al. Safety and antithrombotic efficacy of moderate platelet count reduction by thrombopoietin inhibition in primates. Sci Transl Med. 2010 Jun 23.2(37):37ra45.
77. Hayward CP, Moffat KA, Liu Y. Laboratory investigations for bleeding disorders. Semin Thromb Hemost. 2012 Oct; 38(7):742–752. [PubMed: 23011792]
78. Tullis JL, Pennell RB. Transfusion of specific plasma components. Annu Rev Med. 1968; 19:233–246. [PubMed: 4172726]
79. Berny MA, Munnix IC, Auger JM, Schols SE, Cosemans JM, Panizzi P, et al. Spatial distribution of factor, Xa thrombin, and fibrin(ogen) on thrombi at venous shear. PLoS One. 2010; 5(4):e10415. [PubMed: 20454680]
80. Kolev K, Machovich R. Molecular and cellular modulation of fibrinolysis. Thromb Haemost. 2003 Apr; 89(4):610–621. [PubMed: 12669114]
81. Hedner U, Ezban M. Tissue factor and factor VIIa as therapeutic targets in disorders of hemostasis. Annu Rev Med. 2008; 59:29–41. [PubMed: 17845136]
82. Dellinger RP, Levy MM, Rhodes A, Annane D, Gerlach H, Opal SM, et al. Surviving sepsis campaign: international guidelines for management of severe sepsis and septic shock-2012. Crit Care Med. 2013 Feb; 41(2):580–637. [PubMed: 23353941]
83. Stewart MP, Toyoda Y, Hyman AA, Muller DJ. Tracking mechanics and volume of globular cells with atomic force microscopy using a constant-height clamp. Nat Protoc. 2012 Jan; 7(1):143–154. [PubMed: 22222789]
84. Hanley W, McCarty O, Jadhav S, Tseng Y, Wirtz D, Konstantopoulos K. Single molecule characterization of P-selectin/ligand binding. J Biol Chem. 2003 Mar 21; 278(12):10556–10561. [PubMed: 12522146]
85. Binnig G, Quate CF, Gerber C. Atomic force microscope. Physical review letters. 1986; 56(9):930. [PubMed: 10033323]
86. Garcia R, Herruzo ET. The emergence of multifrequency force microscopy. Nat Nanotechnol. 2012 Apr; 7(4):217–226. [PubMed: 22466857]
87. Nicoletti I, Migliorati G, Pagliacci MC, Grignani F, Riccardi C. A rapid and simple method for measuring thymocyte apoptosis by propidium iodide staining and flow cytometry. J Immunol Methods. 1991 Jun 3; 139(2):271–279. [PubMed: 1710634]
88. McCarty OJ, Jadhav S, Burdick MM, Bell WR, Konstantopoulos K. Fluid shear regulates the kinetics and molecular mechanisms of activation-dependent platelet binding to colon carcinoma cells. Biophys J. 2002 Aug; 83(2):836–848. [PubMed: 12124268]
89. Burdick MM, McCarty OJ, Jadhav S, Konstantopoulos K. Cell-cell interactions in inflammation and cancer metastasis. IEEE Eng Med Biol Mag. 2001 May-Jun;20(3):86–91. [PubMed: 11446216]
90. Colace TV, Tormoen GW, McCarty OJ, Diamond SL. Microfluidics and coagulation biology. Annu Rev Biomed Eng. 2013 Jul 11.15:283–303. [PubMed: 23642241]
91. White-Adams TC, Berny MA, Patel IA, Tucker EI, Gailani D, Gruber A, et al. Laminin promotes coagulation and thrombus formation in a factor XII-dependent manner. J Thromb Haemost. 2010 Jun; 8(6):1295–1301. [PubMed: 20796202]
92. Gutierrez E, Petrich BG, Shattil SJ, Ginsberg MH, Groisman A, Kasirer-Friede A. Microfluidic devices for studies of shear-dependent platelet adhesion. Lab Chip. 2008 Sep; 8(9):1486–1495. [PubMed: 18818803]

93. Hochmuth RM. Micropipette aspiration of living cells. J Biomech. 2000 Jan; 33(1):15–22. [PubMed: 10609514]

94. Betzig E, Trautman JK, Harris TD, Weiner JS, Kostelak RL. Breaking the diffraction barrier: optical microscopy on a nanometric scale. Science. 1991 Mar 22; 251(5000):1468–1470. [PubMed: 17779440]

95. Dawe GS, Schantz J-T, Abramowitz M, Davidson MW, Hutmacher DW. Light microscopy. Techniques in Microscopy for Biomedical Applications. 2006; 2:9.

96. Lakowicz, JR. Principles of fluorescence spectroscopy: Springer. 2009.

97. Phillips KG, Jacques SL, McCarty OJ. Measurement of single cell refractive index, dry mass, volume, and density using a transillumination microscope. Phys Rev Lett. 2012 Sep 14.109(11): 118105. [PubMed: 23005682]

98. Baker SM, Phillips KG, McCarty OJ. Development of a label-free imaging technique for the quantification of thrombus formation. Cell Mol Bioeng. 2012 Dec; 5(4):488–492. [PubMed: 23585817]

99. Baker-Groberg SM, Phillips KG, McCarty OJ. Quantification of volume, mass, and density of thrombus formation using brightfield and differential interference contrast microscopy. J Biomed Opt. 2013 Jan.18(1):16014. [PubMed: 23348747]

100. Popescu G, Park Y, Choi W, Dasari RR, Feld MS, Badizadegan K. Imaging red blood cell dynamics by quantitative phase microscopy. Blood Cells Mol Dis. 2008 Jul-Aug;41(1):10–16. [PubMed: 18387320]

101. Sleep J, Wilson D, Simmons R, Gratzer W. Elasticity of the red cell membrane and its relation to hemolytic disorders: an optical tweezers study. Biophys J. 1999 Dec; 77(6):3085–3095. [PubMed: 10585930]

102. Clauser S, Cramer-Borde E. Role of platelet electron microscopy in the diagnosis of platelet disorders. Semin Thromb Hemost. 2009 Mar; 35(2):213–223. [PubMed: 19408194]

103. Sjollema KA, Schnell U, Kuipers J, Kalicharan R, Giepmans BN. Correlated light microscopy and electron microscopy. Methods Cell Biol. 2012; 111:157–173. [PubMed: 22857928]

104. Pertuy F, Eckly A, Weber J, Proamer F, Rinckel JY, Lanza F, et al. Myosin IIA is critical for organelle distribution and F-actin organization in megakaryocytes and platelets. Blood. 2013 Nov 15.

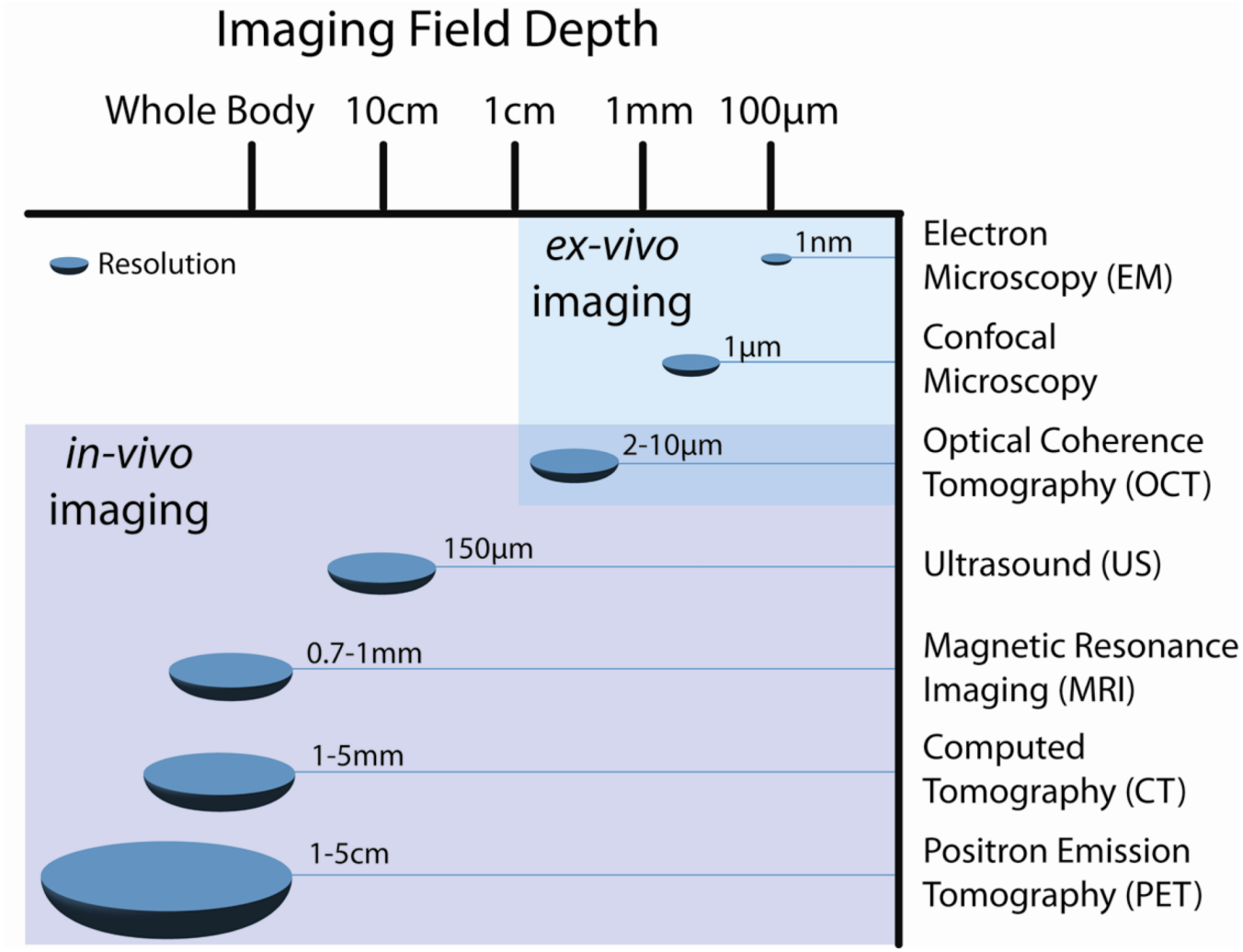

Figure 1.
Resolution and imaging field depth (penetration) of several current imaging modalities are illustrated and compared. Note that resolution decreases as depth increases, rendering modalities such as CT and MRI suitable for imaging whole organs and systems *in vivo* whereas modalities with higher resolution are best suited for *ex vivo* and *in vitro* imaging of smaller structures on the cellular and sub-cellular level. Often two or more modalities are used in tandem to obtain a full understanding of a system or pathology.